Physica A 664 (2025) 130461

Contents lists available at ScienceDirect

Physica A: Statistical Mechanics and its Applications

journal homepage: www.elsevier.com/locate/physa

Beyond traditional metrics: Redefining urban metro network vulnerability with redundancy assessment

Kaveh Rezvani Dehaghani *, Catherine Morency

Department of Civil, Geological and Mining Engineering, Polytechnique Montréal, Québec H3C 3A7, Canada

ARTICLE INFO

Keywords:
Vulnerability analysis
Disruption
Public transportation
Urban Metro Network (UMN)
Redundancy indicators
CDNAN

ABSTRACT

Previous studies have predominantly analyzed Urban Metro Network (UMN) vulnerability from topological and functional perspectives, often neglecting the impact of disruptions on alternative route availability. This research introduces a novel redundancy-based vulnerability analysis, assessing the reduction in travel alternatives following disruptions. The Montreal UMN is used as a case study, utilizing General Transit Feed Specification (GTFS) data from the Montreal Transit Authority and trip data from the 2018 Montreal Origin-Destination survey. Using the open-source platform Transition, we simulate shortest transit routes for each trip, generate alternative routes, and compute travel times. We define one targeted and three random failure scenarios, selected from 100 simulations, to evaluate network vulnerability to various disruption types. Indicators are formulated, calculated, and compared across all scenarios. Each failure scenario involves a sequence of consecutive metro station disruptions, leading to complete network shutdown. Findings reveal that the metro network is significantly more vulnerable to targeted disruptions than random ones. Among all indicators, functional ones related to users' travel time show greater sensitivity to disruption type, be it targeted or random. Vulnerability indicators exhibit the most substantial changes during initial disruptions, highlighting their critical impact. Although traditional approaches (topological and functional) show a direct relationship between the number of disruptions and changes in vulnerability indicators, this is not true for the redundancy-based vulnerability indicator. In this case, the primary determinants are the locations of disrupted stations and the network's geometry, rather than the number of disruptions.

1. Introduction

Metro systems are the mainstay of transit systems and a crucial component of urban transportation infrastructures. Because of its higher speed and reliability, the metro is also considered as an efficient transportation mode [1]. Moreover, due to its beneficial effects on noise reduction, energy conservation, and emission reduction [2], the urban metro system is extremely popular in metropolises. For instance, in Montreal with a population of 1.78 million -embedded in a 4.2 million people metropolitan area, more than 820,000 metro trips are made every day [3], demonstrating the key role that this transit mode plays in this city. The increasing importance of metro systems globally has heightened scholarly interest in examining the vulnerability of Urban Metro Networks (UMNs) over the past decade.

The increasing importance of subway systems worldwide has intensified the need to assess the vulnerability of UMNs.

* Corresponding author.
E-mail addresses: kaveh.rezvani-dehaghani@polymtl.ca (K.R. Dehaghani), cmorency@polymtl.ca (C. Morency).

https://doi.org/10.1016/j.physa.2025.130461
Received 31 July 2024; Received in revised form 11 January 2025; Accepted 15 February 2025
Available online 20 February 2025

Vulnerability, in the context of subway systems, refers to their capacity to maintain service in the face of disruptions. Two principal approaches have traditionally been employed to analyze this vulnerability: topological and functional methods, though they may be referred to under different terminologies. The former, often termed "topological" [4–9], "network-based" or "complex network" [10, 11, 1], or "structural" [12,13], focuses on identifying critical locations within the network—either nodes or links—where disruptions would result in the greatest impact. In contrast, the latter, known as functional analysis [2, 14, 15], serviceability-based analysis, system-based analysis, or transportation performance analysis [16], evaluates transportation characteristics such as node and link capacity, flow, length, and travel time. Serviceability-based methods are complex to apply to public transportation systems. As a result, topological analysis is more commonly used for studying transit network vulnerabilities, while serviceability-based methods are typically applied to road networks. [17].

Previous research has made efforts to combine both topological and functional indicators for conducting systematic vulnerability assessments of transit networks. However, a critical consideration has been overlooked: the role of redundancy. Neither topological nor functional approaches sufficiently address the quantity and quality of alternative routes within the network during disruptions. This gap is particularly important as redundancy plays a key role in maintaining network functionality under failure conditions. To address this issue, the current study proposes a redundancy-based vulnerability assessment framework, using the Montreal UMN as a case study. By gathering relevant data, utilizing appropriate analytical tools, and detailing the methodology, this approach can be extended to other urban metro systems. Fig. 1 presents an overview of the research structure.

This study employs a Block-Based Failure Strategy (BBFS), which accounts for the role of Stations with Direction Change Facilities (SDCFs), enhancing the accuracy of the simulation. Additionally, the research simulates both targeted and random disruptions within

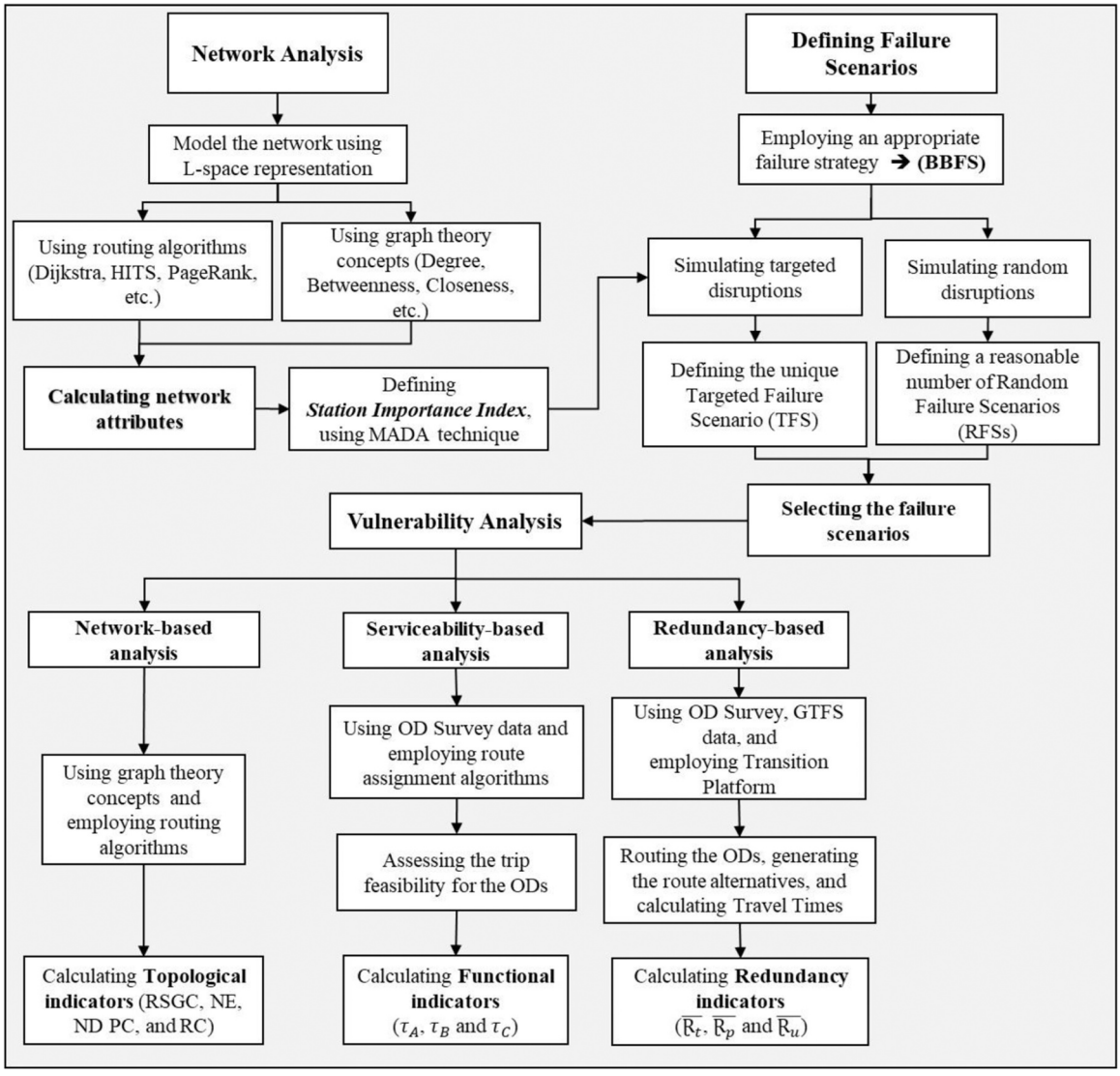

Fig. 1. Methodology Framework.

the subway system, allowing for a comparative analysis of their respective impacts. In addition to introducing a redundancy-based vulnerability assessment, this study makes several other notable contributions:

- Two new indicators namely pure-connectivity and relative-connectivity, are proposed to assess network connectivity. These indicators represent a departure from prior studies that primarily relied on measures such as network efficiency, average path length, or average degree.
- A Multi-Attribute Decision-Making (MADM) technique is applied to develop a Station Importance Index by integrating multiple indicators. This approach contrasts with previous studies that focused on individual indicators to identify critical stations for simulating the targeted disruption.
- This study demonstrates that significant variations can occur among simulated random failure scenarios. Therefore, it is important to conduct iterative simulations of random failures multiple times. By selecting diverse scenarios with varying characteristics, one can ensure a comprehensive understanding of potential outcomes. This approach helps avoid focusing solely on uncommon or rare conditions.

2. Background

The initial definitions of vulnerability in the realm of transportation engineering are traced back to the research by Berdica (2002) [18] and D'Este and Taylor [19]. Berdica defined the vulnerability of transportation networks as *"a susceptibility to incidents that can result in considerable reductions in road network serviceability"*. During the first years of the emergence of this concept in transportation engineering, scholars tried to generalize the initial definition by examining the importance of investigating the vulnerability of transportation networks from different perspectives (see [20], and [21]).

Upon reviewing the related literature, it is obvious that vulnerability assessment studies of transit networks have been classified in various ways. Mattsson and Jenelius [17] introduced an initial categorization into "topological" and "system-based" analyses [17]. Taylor (2017) further delineated these studies into "topologically-based analysis" and "serviceability-based analysis" [22]. Zhang and Zhang (2019) proposed a classification based on "analysis using network topology," "mathematical models," and "accessibility-based analysis," noting that the first two categories are relevant to transit systems [23]. Similarly, Yan et al. (2021) categorized previous research into "topological" and "system performance" analyses [24]. Despite differing terminology used by scholars, these categorizations share fundamental concepts.

Several studies have focused on network topology in vulnerability analysis without considering Origin–Destination (OD) passenger flows. For instance, Meng et al. (2020) analyzed the topological complexity of Urban Rail Transit Networks (URTNs) with multi-line transfer stations, using the Shenzhen Metro as a case study. They developed and compared Space L and Space P models based on multiple evaluation parameters and key node rankings. Their findings indicated that both models exhibited scale-free network characteristics, displaying robustness against random faults but vulnerability to targeted attacks [9]. Similarly, Mussone et al. (2024) examined network robustness through graph theory and introduced a new centrality measure, the Sum of Weighted Distances Index (SWDI). This index quantified the percentage change in travel distances when a node and its edges were disrupted. By comparing SWDI values in both standard and degraded network states, the study identified the edges and nodes most susceptible to performance reductions [25]. In contrast, some studies have exclusively focused on functional indicators, such as demand and travel time, without addressing topological aspects. For example, Zhang et al. (2023) investigated the robustness of URTNs under disruptions using a user equilibrium model with a time compensation mechanism, using the Shanghai subway network as a case study. Their analysis assessed changes in average travel time, link flow, and the demand-supply ratio under three distinct attack modes, identifying critical nodes and links that significantly impacted the network's robustness [26].

More recent studies, however, have incorporated both topological and functional features, including passenger flows, to explore network vulnerability more comprehensively. For example, Du et al. (2020) proposed a novel method for evaluating node significance in metro networks, using the Improved Topological Potential with Entropy (ITPE) model. The ITPE model aggregated multiple centrality measures, with topological entropy determining their weights, to assess node importance. This method's effectiveness was validated through invulnerability measurements, and its application to the Shenzhen Metro system successfully identified critical nodes in terms of both network structure and passenger flow, outperforming traditional undirected and unweighted models [27].

In another study, Zhang et al. (2021) introduced the Integrated Coupled Map Lattices (ICML) model to assess node states and investigate the vulnerability of weighted URTNs under external disturbances. By refining passenger flow into in-flow and out-flow at stations, they introduced a new redistribution rule to analyze cascading failures. Their results revealed a linear relationship between node and edge betweenness, demonstrating that URTNs are highly vulnerable to malicious attacks, with increasing susceptibility as external disturbances grow [16]. Lastly, Song et al. (2024) evaluated the vulnerabilities of rail transit networks (RTNs) through the Chongqing Rail Transit (CRT) system. They developed a network topology model using the spatial L method and analyzed key nodes based on degree, betweenness centrality, network efficiency, and passenger flow volume (PFV). The study identified six node clusters with varying levels of vulnerability and transportation capacity, proposing management strategies to improve planning and safety for RTNs [28].

A review of traditional vulnerability analysis classifications and recent literature reveals ongoing advancements in integrating topological and functional approaches. However, despite these developments, current methods do not consider the impact of disruptions on the frequency and quality of alternative routes within transit systems. This study aims to address this gap by introducing a redundancy-based vulnerability assessment method.

3. Network analysis

The Montreal Urban Metro Network (UMN), comprising four lines—Orange, Blue, Green, and Yellow—along with 68 stations, is selected as the case study for this research. Fig. 2 provides additional details about the Montreal UMN. Following the principles of complex network theory and L-space representation [29], this network is modeled as an undirected graph $G = (V,E)$, where $V = \{v_i | i = 1, 2, 3 \ldots N\}$ represents the set of nodes, and $E = \{e_{ij} | v_i, v_j \in V\}$ represents the set of edges. In this model, stations are considered as nodes, while the lines connecting them are represented as edges.

The importance of stations within the metro system can be determined through two main approaches: functional features, such as boarding and alighting volumes, and topological features, such as network centrality. While these two methods are conceptually distinct, the functional importance of stations can fluctuate depending on factors like the time of day, whereas topologically important stations remain consistent. Although both approaches provide valuable insights, this research, like the majority of studies in this field, focuses on the network's topological features. However, unlike prior research that typically relied on a single indicator (often degree or betweenness centrality), this study introduces multiple independent indicators to assess the topological importance of stations. Each indicator serves as a criterion for determining the Station Importance Index.

3.1. Degree centrality

The *degree centrality* of v_i is shown by $C_D(v_i)$ which is the total number of edges connected to v_i.

$$C_D(v_i) = \deg(v_i) = \left|\{v_j \in V : (v_i, v_j) \in E\}\right| \tag{1}$$

Where v_j represents any other node in the graph that is connected to v_i; V is the entire set of nodes in the network; E represents the set of edges in the network.

3.2. Betweenness centrality

The *betweenness centrality* of v_i is shown by B_i which is the proportion of shortest paths passing through node i among all the shortest paths of the graph.

$$B_i = \sum_{u \neq v \neq 1} \frac{\tau_{uv}(i)}{\tau_{uv}} \tag{2}$$

Where: $\tau_{uv}(i)$ represents the number of shortest paths passing through node i between node u and node v, and τ_{uv} represents the number of shortest paths between node u and node v. These can be calculated in an undirected network using Eq. 3:

$$\tau_{uv} = \frac{(N-1) \times (N-2)}{2} \tag{3}$$

Where N is the total number of nodes in an UMN

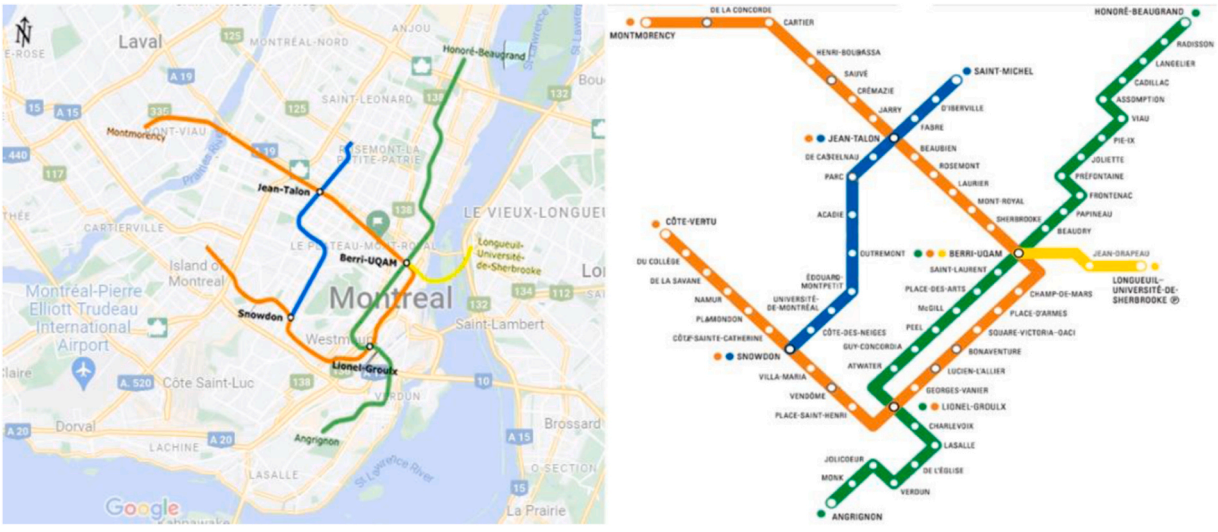

Fig. 2. Montreal metro network [3].

3.3. Closeness centrality

In an UMN, the station's *closeness centrality* is determined by taking the reciprocal of the lengths of its shortest paths to all other stations in the network. In a rail network, nodes that have a higher closeness centrality are located closer to one another. This indicates that a trip is convenient because the total cost of traveling between nodes is the shortest.

$$CC_i = \frac{N-1}{\sum_{j \in V,\ i \neq j} d_{ij}} \tag{4}$$

Where d_{ij} is the average length of the shortest path between node i and j.

3.4. PageRank

This indicator evaluates the importance of nodes in a graph by considering the recursive relationship between significant nodes and the significance of the nodes around them. In a metro network, PageRank identifies the most important stations by considering both the number of direct connections a station has (i.e., the degree of the station) and the importance of the stations it connects to. Stations with many well-connected neighboring stations (such as major transfer hubs) will have higher PageRank values, reflecting their critical role in network connectivity and passenger flow.

$$PR_{v_i} = \frac{1-\lambda}{N} + \lambda \sum_{v_j \in \Gamma(v_j)} \frac{PR(v_j)}{\deg(v_j)} \tag{5}$$

Where v_i is the node for which the PageRank is being calculated, v_j represents the neighboring nodes of v_i, $\Gamma(i)$ is the set of neighbors of node v_i, and λ is the damping coefficient which is generally 0.85 [30], representing the probability of continuing to follow edges.

3.5. Hub/Authority

Hubs and Authorities were inspired by a specific observation about web page development during the early stages of the internet. Some websites, known as hubs, served as extensive directories that aggregated a diverse range of resources, directing users to other authoritative pages rather than providing authoritative information themselves. In the context of the UMN, a good authority is a station linked by many different hubs, while a good hub is a station that links to many other stations. The Hyperlink-Induced Topic Search (HITS) algorithm is employed to calculate hub and authority scores [31]. In an undirected graph, the Hub and Authority scores in the HITS algorithm are iteratively calculated, with each node's score depending on the scores of its neighbors. In each iteration, the Hub score of a node is updated based on the current Authority scores of its connected nodes, and vice versa, the Authority score is updated using the Hub scores of the neighboring nodes. This iterative process continues until the scores converge, reflecting the mutual reinforcement between Hub and Authority values.

$$h_i = \sum_{j \in \Gamma(v_i)} a_i \tag{6}$$

$$a_i = \sum_{j \in \Gamma(v_i)} h_i \tag{7}$$

Where h_i is Hub score for node v_i, and a_i is Authority score for node v_i

3.6. Eigenvector centrality

This indicator illustrates how nodes influence each other within a network, with a node's score being more significantly increased by connections from other high-scoring nodes. A node that is connected to many nodes with high scores will have a higher eigenvector centrality. The algorithm computes the eigenvector corresponding to the largest absolute eigenvalue, typically using the power iteration method. In each iteration, the centrality score of each node is updated based on the scores of its neighbors, and this process continues until convergence.

The Eigenvector centrality for node is defined as the solution to the following equation:

$$Ax = \mu x \tag{8}$$

Where A is the adjacency matrix of the graph, $x = (x_1, x_2, \ldots, x_n)$ is the vector of eigenvector centralities for all nodes, x_i represents the centrality of node v_i, and μ is the principal eigenvalue associated with the adjacency matrix.

4. Failure scenarios

In this section, two key concepts must be defined: disruption and failure scenarios. In this research, a disruption is characterized as

an accident, incident, or event occurring within a metro station. Depending on the network topology, a single disruption may impact either the affected station alone or a group of stations, necessitating the simulation of such disruptions. To simulate disruptions, a failure strategy must be employed. Furthermore, a failure scenario involves a sequence of consecutive disruptions at metro stations, ultimately resulting in the complete collapse of the Urban Metro Network (UMN).

4.1. Failure strategy

The Block-Based Failure Strategy (BBFS) employed in this study builds upon the previously established concept of turn-back operations [32] but introduces specific enhancements tailored to urban rail networks. While both approaches share a common foundation in modeling disruptions and their cascading impacts, BBFS distinguishes itself by defining the concept of a "block." In BBFS, a block refers to a segment of consecutive regular stations situated between two consecutive Stations with Direction-Change Facilities (SDCFs). Additionally, BBFS incorporates a nuanced categorization of SDCFs, distinguishing between fully equipped SDCFs, which facilitate direction changes for both paths (both directions), and semi-equipped SDCFs, which provide direction-changing capabilities for only one path.

In BBFS, the general rule is that the failure of a regular station results in the failure of the entire block to which it belongs, and the disruption of an SDCF affects all connected blocks. However, as illustrated in Fig. 3, semi-equipped SDCFs can lead to more localized impacts. For example, station 52 is a semi-equipped SDCF that provides direction-changing capabilities only to the right path. Thus, if a station on the left side of station 52 (e.g., station 51 or 50) is disrupted, only block 18 will be affected, and stations 50 and 51 will be disrupted. Conversely, if a station on the right side of station 52 is disrupted, both blocks 18 and 19 will be out of service. These adaptations render BBFS a specialized extension of the turn-back operation concept, offering greater applicability to the structural and operational complexities of urban rail systems. Further details about the Montreal UMN, which consists of 24 blocks, are provided in Fig. 3.

4.2. Targeted disruptions

In earlier studies, targeted failure scenarios were often simulated by selecting nodes for removal based on descending order of degree or betweenness centrality. However, in this research, we introduced a Station Importance Index as the primary criterion for selecting the most crucial station. This index incorporates various centrality-related attributes of the network simultaneously, providing a ranking of station importance based on centrality metrics. The station identified with the highest station importance according to this index is chosen for targeted disruptions in our approach.

4.3. Calculating the station importance index

In this study, we applied the Technique for Order of Preference by Similarity to Ideal Solution (TOPSIS) [33], a method of Multi-Attribute Decision Making, to identify the most significant station within a specified network context. Our analysis considered 68 alternatives (station) and 7 network-centrality attributes under normal conditions. The importance of stations was assessed using

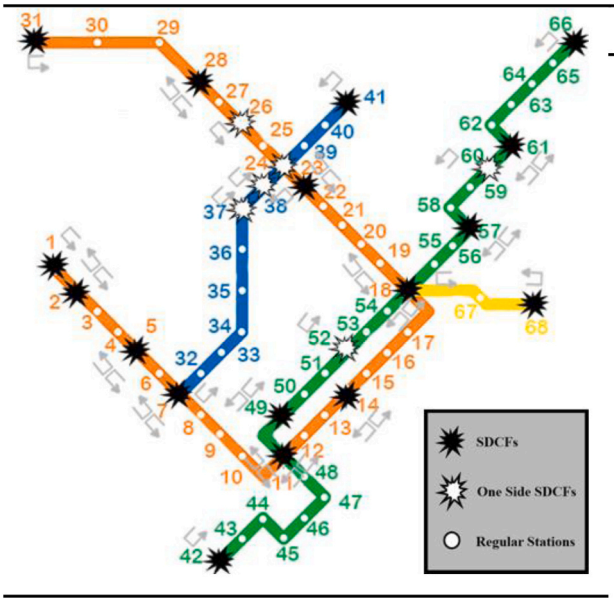

Block ID	Associated Stations
1	1,2
2	2,3,4,5
3	5.6,7
4	7,8,9,10,11
5	11,12,13,14
6	14,15,16,17
7	18,19,20,21,22,23
8	23,24
9	24,25,26
10	26,27,28
11	28,29,30,31
12	7,32,33,34,35,36,37
13	37,38
14	38,24
15	24,39,40,41
16	42,43,44,45,46,47,48,11
17	11,49
18	49,50,51,52
19	52,53,54,18
20	18,55,56,57
21	57,58,59,60

Fig. 3. Montreal UMN blocks.

various logics and algorithms associated with these attributes. To facilitate the TOPSIS methodology, attribute weighting was implemented using Shannon's entropy method [34], as elaborated in the following discussion.

A decision matrix is needed in the first step, in which the elements must match the values of the aforementioned attributes of each node (stations). Hence, in the decision matrix $[X]_{m*n,}$ m represents the number of choices (stations) and n is the value of attributes.

$$X = \begin{bmatrix} X_{11} & X_{12} & \dots & X_{1N} \\ X_{21} & X_{22} & \dots & X_{2N} \\ \dots & \dots. & \dots & \dots \\ X_{M1} & X_{M2} & \dots & X_{MN} \end{bmatrix}$$

The second step deals with normalising the decision matrix. Because of the potential for a large difference between the value ranges of different attributes and the variations in the measurement units, the values of the attributes should be normalized. For this, Eq. 6 is employed.

$$p_{ij} = \frac{X_{ij}}{\sum_{i=1}^{n} X_{ij}} \tag{6}$$

The next step is related to the computation of the entropy of attributes using the Eq. 7.

$$E_j = \quad -k \quad \sum_{i=1}^{m} p_{ij} \ln p_{ij} \tag{7}$$

$$\text{Where} k = \frac{1}{\ln(m)}$$

The third step entails computing the attributes' weights using the entropy concept:

$$w_j = \frac{1 - E_j}{\sum_{j=1}^{n} (1 - E_j)} \tag{8}$$

The ranking results of the node (station) importance should be established by the TOPSIS approach after determining the weight of the attributes. Five steps must be taken in this regard.

First, determine the normalized matrix using Eq. 9:

$$\overline{X}_{ij} = \frac{X_{ij}}{\sqrt{\sum_{j=1}^{n} X_{ij}^2}} \tag{9}$$

Second, determine the weighted normalized matrix:

$$V_{ij} = \overline{X}_{ij} \quad \times \quad w_j \tag{10}$$

Third, calculate the ideal best and ideal worst value:

$$\begin{cases} v^+ = \max(V_1^+, \quad V_2^+ \dots, \quad V_p^+) \\ v^- = \min(V_1^-, \quad V_2^- \dots, \quad V_p^-) \end{cases}$$

Fourth, calculate the Euclidean distance from the ideal best and ideal worst:

$$S_i^+ = \sqrt{\sum_{j=1}^{m} (V_{ij} - V_j^+)^2} \tag{11}$$

$$S_i^- = \sqrt{\sum_{j=1}^{m} (V_{ij} - V_j^-)^2} \tag{12}$$

Fifth, determine the performance score:

$$P_i = \frac{S_i^-}{S_i^+ + S_i^-} \tag{13}$$

A summary of the required steps to calculated station importance is given in Fig. 4.

Table 1 provides detailed insights into the station selection process during the targeted failure scenario. For each network scenario, the weights of seven criteria used to identify the most important station are computed. The total weight of criteria in each table row

sums up to one. Therefore, while considering the impact of each criterion (based on its weight) in identifying the most important station, Table 1 highlights the most influential criterion in each network scenario (i.e., the criterion with the highest weight).

For instance, in the normal state (no disruption), closeness centrality emerges as the most influential indicator, with "Berri-UQAM" (station #18) identified as the highest in importance. Following the first simulated disruption (removal of the most important station), according to BBFS (Block-Based Failures Strategy), seventeen stations within the same blocks as Berri-UQAM would be out of service. After each disruption simulation, the network undergoes analysis, recalculating and reweighting all indicators.

Based on the details presented in Table 1 regarding successive targeted disruptions, the network is predicted to collapse after nine targeted disruptions. Thus, the Corresponding Disruption Number to the Annihilation of the Network (CDNAN) in the targeted failure scenario is 9.

4.4. Random disruptions

Using random numbers to select stations for removal is a common method for simulating random failure scenarios. However, this approach can sometimes produce outputs that create unusual graph states that differ significantly from actual conditions. For instance, all randomly selected nodes might be consecutive, located at the beginning or end of lines, or at transfer stations.

To mitigate the impact of these outcomes, we conduct the simulation 100 times and adopt the most frequently occurring scenario as the realistic random scenario. This iterative process helps to reduce the influence of anomalous outcomes and ensures that the simulated random failures better represent typical or expected scenarios within the network graph.

Fig. 5 illustrates that among 100 simulated random scenarios, the most frequently repeated CDNAN is 17, occurring 27 times. This scenario is referred to as Realistic Random Failure Scenarios (RRFS). In one scenario, the CDNAN is 11, characterized as the Pessimistic Random Failure Scenario (PRFS). Conversely, in the most optimistic case, the CDNAN is 22, representing the Optimistic Random Failure Scenario (ORFS). These different scenarios provide insights into the range of potential outcomes resulting from random failure simulations.

4.5. Selected scenarios

In this study, we identify one Targeted Failure Scenario (TFS) with the lowest possible Corresponding Disruption Number to the Annihilation of the Network (CDNAN) as the worst-case scenario. Additionally, we select three random failure scenarios corresponding to the lowest (PRFS), the most frequent (RRFS), and the highest (ORFS) CDNAN among 100 simulated scenarios.

It is important to note that the CDNAN values corresponding to TFS, PRFS, and ORFS are unique. However, since CDNAN equals 17 in 27 simulated scenarios, the RRFS used in our analysis was randomly selected from these 27 scenarios. Table 2 provides detailed information about the sequence of selecting stations in each scenario, namely how stations are chosen during the simulation of targeted and random failure scenarios to assess network resilience and vulnerability.

5. Vulnerability analyses

5.1. Network-based analysis using topological indicators

Topological indicators are primarily used to evaluate network connectivity. Previous studies have employed various metrics, such as the Relative Size of Giant Components, Network Efficiency, and Network Diameter, to assess connectivity. In addition to these conventional indicators, this research introduces two novel metrics: Pure Connectivity and Relative Connectivity. These new indicators are based on two factors: the Size of the Giant Component (SGC) and the Number of Connected Components (NCC). The SGC directly

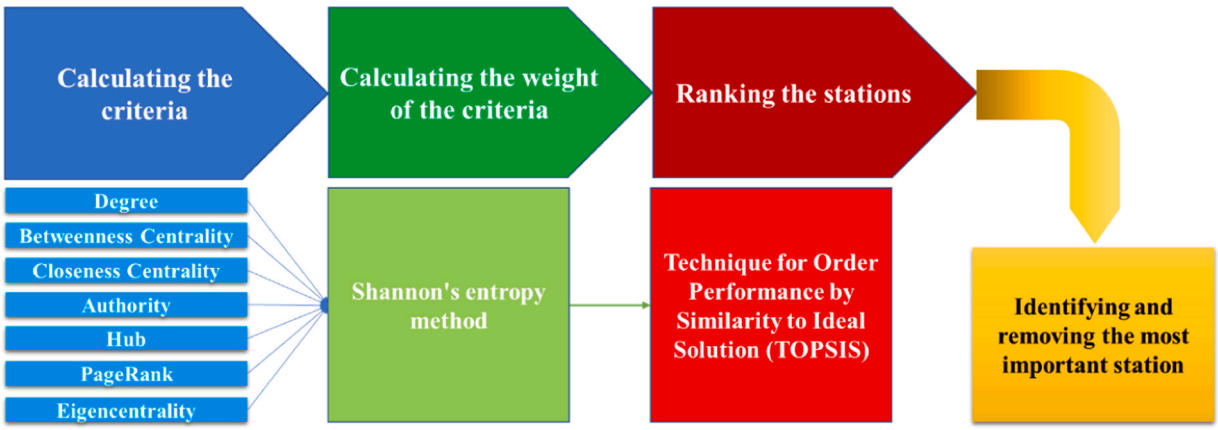

Fig. 4. Schema of steps to identify the most important station.

Table 1
Order of selected stations in the targeted failure scenario.

Network situation	Criteria weight							Code and Name of the Purposefully Selected Station(Station with highest importance index)
	Degree	Closeness centrality	Betweenness centrality	Authority	Hub	Page Ranks	Eigen centrality	
N.S	0.09	0.29	0.16	0.11	0.16	0.09	0.11	18 (Berri-UQAM)
D#1	0.10	0.19	0.24	0.09	0.14	0.10	0.13	11 (Lionel-Groulx)
D#2	0.08	0.20	0.25	0.12	0.18	0.07	0.11	24 (Jean-Talon)
D#3	0.23	0.08	0.14	0.18	0.18	0.13	0.06	61 (Viau)
D#4	0.24	0.12	0.13	0.14	0.17	0.14	0.07	4 (Namur)
D#5	0.20	0.11	0.17	0.15	0.15	0.12	0.10	58 (Prefontaine)
D#6	0.19	0.13	0.15	0.16	0.16	0.11	0.10	29 (Cartier)
D#7	0.13	0.20	0.13	0.11	0.20	0.11	0.13	6 (Cote-Sainte-Catherine)
D#8	0.14	0.14	0.14	0.14	0.14	0.14	0.14	1 (Cote-Vertu)

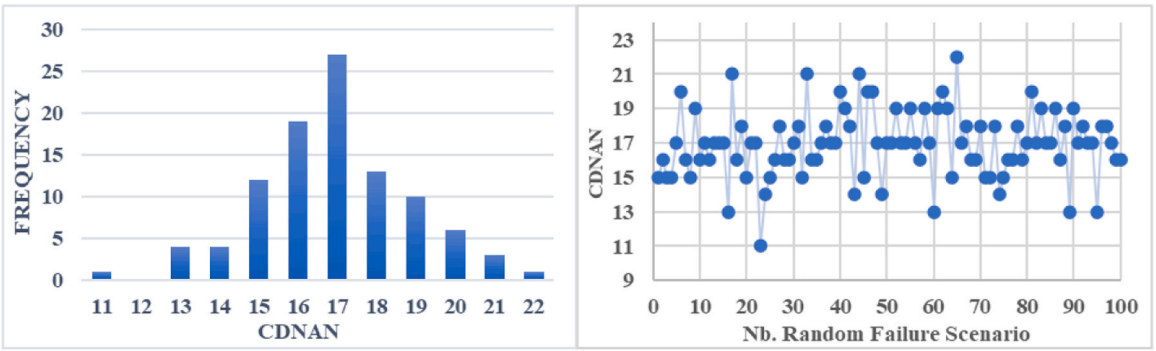

Fig. 5. Details of simulated random failure scenarios.

reflects network connectivity, with a larger SGC indicating that more stations remain connected, signifying greater overall cohesion. In contrast, NCC has an inverse relationship with connectivity. As NCC increases, the network fragments into more isolated components, reducing the relative connectivity of the remaining network compared to the original. Thus, while SGC measures the strength of connectivity, NCC reflects the degree of network fragmentation.

Relative Size of the Giant Component (RSGC)

This indicator is defined as the order ratio of the largest connected subgraph of the network to the original graph. The *RSGC* is calculated using Eq. 14:

$$RSGC = \frac{N'}{N_O} \tag{14}$$

Where N represents the order of the giant component (the largest connected subgraph after the disruption), and $N_O$is the node number of the original graph.

Network Efficiency (NE)

This indicator, which is also called global efficiency, is used to assess the efficiency of the entire network. It is obvious that lower values for shortest paths suggest a greater efficiency, showing the shortest paths have an adverse relationship to network efficiency. The *NE* is given as Eq. 15 [35]:

$$E = \frac{\sum_{i \neq j} \frac{1}{d_{ij}}}{N(N-1)} \tag{15}$$

Where d_{ij} is the shortest distance between v_i and v_j,

Network Diameter (ND)

This indicator is defined as the maximum distance between two nodes in the giant component, calculated using Eq. 16:

$$ND = \max\{d_{ij}\} \tag{16}$$

Pure Connectivity (P.C)

This indicator quantifies the average number of directly connected stations in the network and is formulated as:

Table 2
Additional information on failure scenarios.

Scenario	Description	Nb. Disruption																				
		1	2	3	4	5	6	7	8	9	10	11	12	13	14	15	16	17	18	19	20	21	22
TFS	CSS	18	11	24	61	4	58	29	6	1													
	NRS	51	36	21	15	13	9	5	2	0													
PRFS	CSS	7	26	19	40	11	63	1	18	60	31	4											
	NRS	51	53	48	44	34	29	27	12	7	3	0											
RRFS	CSS	39	31	2	49	56	28	20	7	13	45	52	18	63	38	24	61	59					
	NRS	65	62	58	55	53	51	47	36	34	26	23	16	11	9	5	4	0					
ORFS	CSS	33	8	51	7	29	61	19	45	52	59	49	16	39	57	28	12	4	68	37	1	38	26
	NRS	63	60	58	56	53	47	43	36	33	30	29	26	23	20	18	14	11	8	7	5	4	0

CCS: Code of the Selected Station
NRS: Number of Remaining Stations

$$P.C = \frac{\sum_{i=1}^{N_A} |N_G(i)|}{N_A - 1} \tag{17}$$

Where $|N_G(i)|$ denotes the number of adjacent nodes to station i calculated as the sum of the entries in the i^{th} row of the adjacency matrix. N_A is the total number of accessible stations in the network.

Computing $P.C$ requires summing the adjacency matrix rows, which has a complexity of $O(N^2)$ for dense networks but reduces to

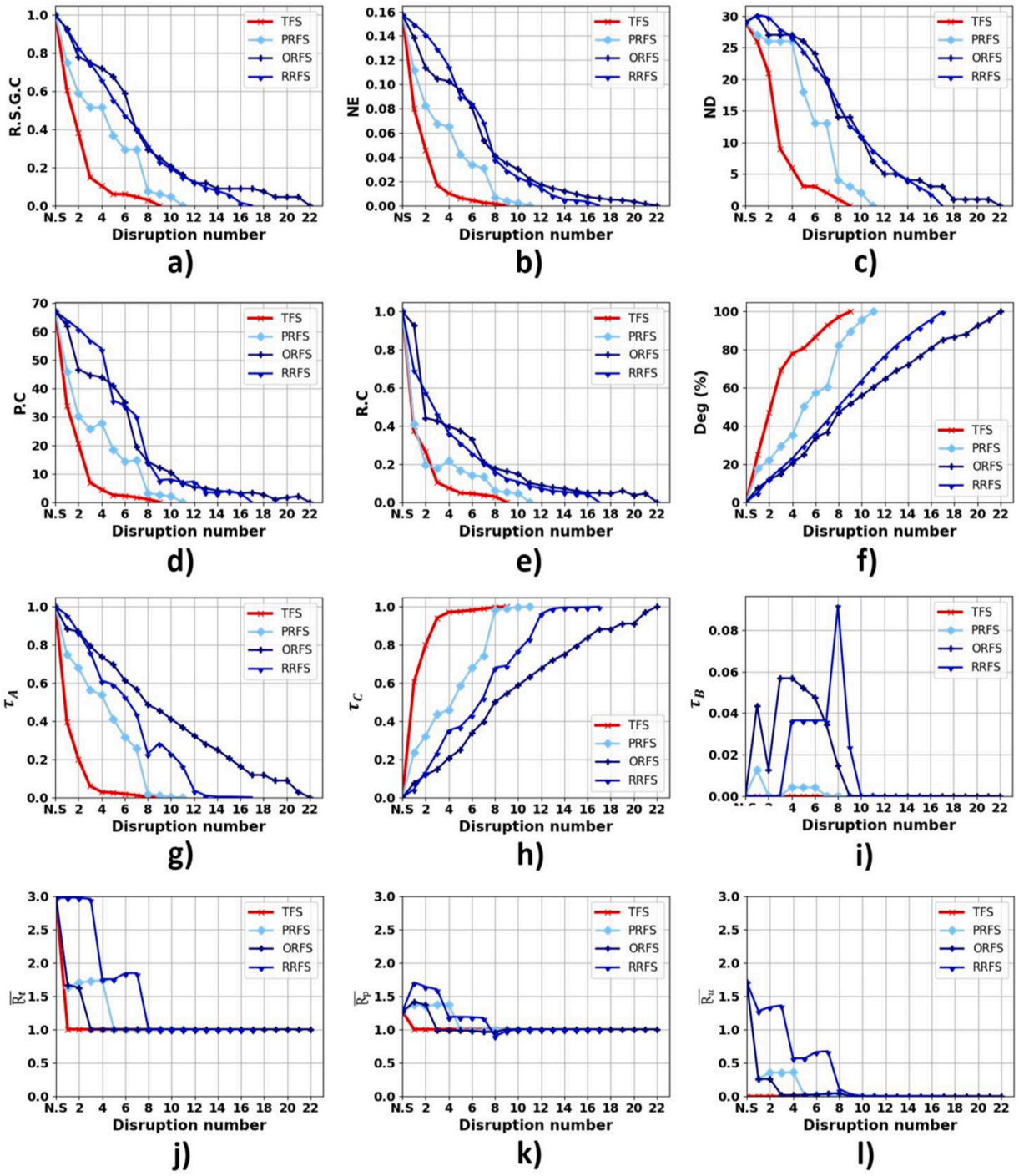

Fig. 6. Results of network-based vulnerability analysis.

$O(E)$ for sparse networks, where E is the number of edges. Thus, this indicator is computationally feasible for metro networks, especially when leveraging sparse matrix representations.

While analyzing very large networks may demand computational optimizations, *P.C* is straightforward to implement for metro systems with manageable sizes. Its simplicity and reliance on fundamental network properties make it a practical and reliable indicator for understanding network connectivity under disruptions. These advantages outweigh the potential challenges in its application to more complex or large-scale systems**.**

Relative Connectivity (R.C)

This indicator evaluates the proportion of accessible stations in the disrupted network relative to its pre-disruption state and is defined as:

$$R.C = \frac{N_A}{N.C.C \quad \times N} \tag{18}$$

Where *N.C.C* represents the number of the connect components.

The computation of *R.C* requires identifying the connected components of the disrupted network. This task is performed using graph traversal algorithms like Depth-First Search (DFS) or Breadth-First Search (BFS), with a complexity of $O(N + E)$, where N and E are the number of nodes and edges, respectively. Although connected component analysis can become more resource-intensive for larger networks, it remains feasible for most metro systems. The indicator provides significant insights into network fragmentation, enabling clear comparisons between pre- and post-disruption scenarios. Its ability to capture the level of disconnection makes *R.C* a valuable indicator for urban transit systems, where ensuring accessibility is critical.

Generally speaking, *P.C* indicates the present situation of the network after each disruption in terms of connectivity, while *R.C* mainly indicates the extent of fragmentation of the network after each disruption compared to the normal state.

5.1.1. Vulnerability analysis

The network-based vulnerability assessment in this research incorporates topological and connectivity vulnerability indicators, along with a novel foolproof indicator known as Cumulative Degradation percentage (*C.Deg*%). This indicator quantifies the ratio of out-of-service stations to the total number of accessible stations in the normal state. *C.Deg*% provides a straightforward measure of network degradation, reflecting the proportion of stations that are unavailable relative to the total number of stations accessible under normal conditions.

5.1.1.1. Normal state. The initial network analysis reveals that the network comprises a single connected graph, signifying that all stations are part of the same component. Consequently, *RSGC* equals 1. The original network efficiency (*NE*) is calculated as 0.157, indicating a network that is not well-connected. The longest shortest path in the graph, with a length of 29 links, corresponds to the route connecting station #1 (Côte-Vertu) to station #66 (Honoré-Beaugrand), denoted as *ND*, which equals 29. The shortest path lengths used in computing NE and ND are determined using the Dijkstra algorithm [36] implemented in Python. Moreover, based on the above defined indicators, $P.C = 67$, meaning that in normal state, each station is connected to 67 stations, and relative connectivity (*R.C*) equals 1.

5.1.1.2. After the disruptions. As depicted in Fig. 6**-a**, the rate of Relative Size of Giant Component (RSGC) decline in the Targeted Failure Scenario (TFS) is notably more pronounced compared to random failures, indicating rapid network destabilization under targeted disruptions. Additionally, a comparison among the three random failure scenarios reveals that the Optimistic Random Failure Scenario (ORFP) and the Realistic Random Failure Scenario (RRFP) exhibit similar decreasing trends in RSGC, suggesting that changes in RSGC are slower in scenarios with larger Corresponding Disruption Number to the Annihilation of the Network (CDNAN) than those with smaller CDNAN.

Initial disruptions, particularly targeted ones, induce the most significant and swift reduction in Network Efficiency (*NE*) (Fig. 6**-b**). Comparisons between scenarios demonstrate a 50 % decrease in *NE* after the first disruption in TFS (from 0.157 to 0.080), whereas *NE* in RRFS shows less than 5 % reduction after the first disruption, highlighting *NE*'s sensitivity to targeted disruptions. Furthermore, it is noteworthy that across all scenarios, initial disruptions exert a more pronounced effect on *NE* reduction compared to subsequent disruptions.

The trend of Network Diameter (*ND*) changes in TFS notably differs from random failure scenarios, indicating a more rapid decline in node closeness and network accessibility under targeted disruptions (Fig. 6**-c**). Moreover, the steepness of the tangent gradient on the TFS diagram suggests that *ND* changes due to initial disruptions are more substantial than subsequent disruptions, whereas random failure scenarios, particularly RRFS and ORFS, show no significant variance in *ND* changes.

Fig. 6**-d** illustrates a distinct decrease in Pure-Connectivity (*P.C*) during the initial disruptions within TFS. This reduction amounts to approximately 90 % after the third disruption. In contrast, random disruptions (especially RRFS and ORFS) exhibit different trends, indicating a higher sensitivity of network connectivity to targeted disruptions. As expected, the initial disruptions in TFS have a greater impact on reducing *P.C* compared to subsequent disruptions across all scenarios. There is no significant difference observed in *P.C* changes during the final disruptions in these scenarios.

In Fig. 6**-e,** both targeted and random failure scenarios exhibit a similar trend of Robustness Coefficient (R.C) decrease, notably declining during initial disruptions. However, this trend is more pronounced in targeted disruptions than random ones (especially in RRFS and ORFS), underscoring targeted disruptions' greater impact on reducing network connectivity.

Cumulative Degradation percentage (*C.Deg*(%)), representing network deterioration, shows a steep tangent gradient in the TFS diagram, indicating the sharpest increase in *C.Deg*(%) under targeted disruptions. After the first disruption, 25 % of stations are out-of-service in TFS, whereas in RRFS, *C.Deg*(%) remains under 5 % after the first disruption (Fig. 6-**f**).

Key observations from this network-based analysis include:

1. The network is significantly more vulnerable to targeted disruptions.
2. Initial disruptions exert a greater impact on network vulnerability across all scenarios.
3. Networks with lower CDNAN exhibit higher vulnerability.
4. Meaningful differences in connectivity reduction rates are observed between newly introduced indicators (*R.C* and *P.C*) and the previously used (*ND*), particularly when comparing TFS to PRFS, suggesting that *ND* alone does not offer a precise interpretation of connectivity.

5.2. Serviceability-based analysis using functional indicators

In this section, we analyze the feasibility of users' travel under different failure scenarios. To assess this, we employ three indicators inspired by [37] that show the number of feasible trips before and after the disruptions.

$$\tau_A = \frac{T_i^A}{T_O} \tag{19}$$

$$\tau_B = \frac{T_i^B}{T_O} \tag{20}$$

$$\tau_C = \frac{T_i^C}{T_O} \tag{21}$$

Where: T_i^A represents the number of trips that still utilize the initial route (the shortest possible path) after the i^{th} disruption, T_i^B denotes the number of trips that had to use longer routes after the i^{th} disruption occurred, T_i^C denotes the number of trips that could not be completed after the i^{th} disruption., and T_O is the total number of trips done before the disruption occurred (in the normal state).

It should be noted that $(T_i^A + T_i^B)$ represents the possible satisfied demand after the i^{th} disruption, and T_i^C represents the unsatisfied demand after the i^{th} disruption. This is also clear that $T_O = T_i^A + T_i^B + T_i^C$

To compute the indicators mentioned, considering travel demand is necessary. To achieve this, we utilized data from the 2018 Montreal Origin-Destination survey. After data processing and weighting the data, we identified a total of 350,879 trips (after data expansion) exclusively using the metro system, which serves as the dataset for this research. Subsequently, to evaluate trip feasibility, we implemented a network graph in Python to validate the existence of routes between nodes (stations).

5.2.1. Vulnerability analysis

5.2.1.1. Normal state. Since in the normal state all trips are feasible using the shortest path, it is obvious that $T_O = T_0^A = 1$, and $T_0^B = T_0^C = 0$.

After the disruptions

Based on Fig. 6-**g** and Fig. 6-**h**, values of τ_A and τ_C reveal that the most significant reduction in satisfied demand is associated with the Targeted Failure Scenario (TFS). After the first, second, and third disruptions in TFS, τ_C reaches 62 %, 82 %, and 95 % respectively, indicating pronounced vulnerability of network serviceability to targeted disruptions. This vulnerability is further supported by comparing the tangent gradient of the TFS diagram with random scenarios in τ_A and τ_C. Among the three random failure scenarios, the Pessimistic Random Failure Scenario (PRFS) exhibits a higher decrease rate in satisfied demand, suggesting that each disruption has a more substantial impact on satisfied demand in this scenario compared to the other two random failure scenarios.

Furthermore, the τ_A and τ_C diagrams reveal that in failure scenarios with smaller Corresponding Disruption Number to the Annihilation of the Network (CDNAN), the initial disruptions have a more significant impact on satisfied demand (number of feasible trips on the subway network). As CDNAN increases, the curvature of the τ_A and τ_C diagrams decrease. For instance, in the Optimistic Random Failure Scenario (ORFS), the relationships between τ_A and τ_C with the number of disruptions are approximately linear, indicating that all disruptions have a nearly equal impact on reducing satisfied demand.

According to Fig. 6-**i**, in the TFS, after the first disruption, only one route remains between each possible origin and destination in the network. Consequently, no user can continue his trip by accepting a longer route after the disruption. In such scenarios, the following relationships hold after each disruption: $\tau_B = 0$, $\tau_A = 1\text{-}\tau_C$. In contrast, among random failure scenarios, after some initial disruptions, it is observed that some users can still continue their metro travels by accepting longer routes after the disruption. The frequency of such trips in each scenario is directly related to the CDNAN, meaning that higher CDNAN values in a scenario correspond to a higher number of passengers who can continue traveling by metro after disruptions (provided they accept longer routes).

The key findings of the serviceability-based analysis are summarized as follows:

1. Network serviceability is significantly more vulnerable to targeted disruptions compared to random disruptions.
2. Initial disruptions have a greater impact on network serviceability across all scenarios.
3. Scenarios with a lower Critical Degree of Network Affiliation Number (CDNAN) exhibit higher vulnerability in network serviceability.
4. Comparing the tangent gradient of the diagrams reveals a more significant difference between targeted and random failure scenarios in serviceability-based analysis compared to network-based analysis. This suggests that functional indicators are more sensitive to the type of disruption than topological and connectivity indicators.

The sensitivity of indicators to disruption type reflects their susceptibility to decline during different failure scenarios, with greater susceptibility indicating higher sensitivity.

5.3. Redundancy-based analysis

The redundancy of a transportation network is evaluated based on the number of available routes between stations, with each route considered a simple path where no node is traversed more than once. In this study, data from the 2018 Montreal Origin-Destination survey and General Transit Feed Specification (GTFS) from the STM [3] website were utilized. To compute trip routes, generate alternatives, and calculate associated travel times, the Transition Platform—a Polytechnique Montreal-developed open-source software (www.transition.city)—was employed. This platform leverages the Connection Scan Algorithm (CSA) for transit route generation.

To determine total travel time for each trip, several components were considered, including total vehicle time, waiting time, access and egress time, and transfer walking time where applicable. The study applied a maximum access travel time of 10 minutes and a maximum egress travel time of 15 minutes, with a 10-minute limit on access time during transfers. These parameters allowed the calculation of travel times for 308,721 trips, representing 88 % of the total trips captured in the dataset.

5.3.1. Quality of alternatives

This study evaluates route alternatives within the Montreal metro network by considering both the availability of multiple routes between origin-destination (OD) pairs and the quality of these routes in terms of travel time. A key focus is on defining a quality threshold based on trip duration. This threshold distinguishes acceptable from unacceptable route alternatives. Based on observations of Montreal metro users, it is hypothesized that passengers are unlikely to consider alternate routes if the travel time is more than twice that of their shortest available option.

For instance, Fig. 7 depicting theoretical routes between station #1 (Côte-Vertu) and station #13 (Lucien-L'Allier). Four routes are identified with durations of 24, 45, 52, and 61 minutes (during workdays at 8:00 AM). The shortest path between these stations takes 24 minutes. According to the defined quality threshold, an acceptable alternative route should have a duration less than twice the time of the shortest path in normal conditions (i.e., before disruptions). In this specific example, the second-best route option has a duration of 45 minutes, which is less than twice the duration of the shortest path (48 minutes). Therefore, it qualifies as an acceptable alternative. Conversely, the third and fourth route options exceed this threshold, with durations of 52 and 61 minutes respectively, and are therefore deemed unacceptable alternatives based on the defined quality criteria.

5.3.2. Redundancy indicators

To introduce the redundancy indicators, the following concepts for each OD pair must be defined:

Theoretical Redundancy (R_t): The total number of available routes (simple paths).

Acceptable Redundancy (R_p): The number of routes meeting the predefined quality threshold.

Unacceptable Redundancy (R_u): The number of routes failing to meet the quality threshold.

Consequently, for each OD pair, a numerical value is assigned to each of the aforementioned indicators. Generally, it holds that $R_t = R_p + R_u$.

A specific subset of R_u represents unsatisfied demand during disruptions (when $R_t > 0$ and $R_p = 0$). This occurs when both the origin and destination remain physically accessible and theoretically connected, but the available route(s) fail to meet the quality threshold. In this research, two types of unsatisfied demand are defined:

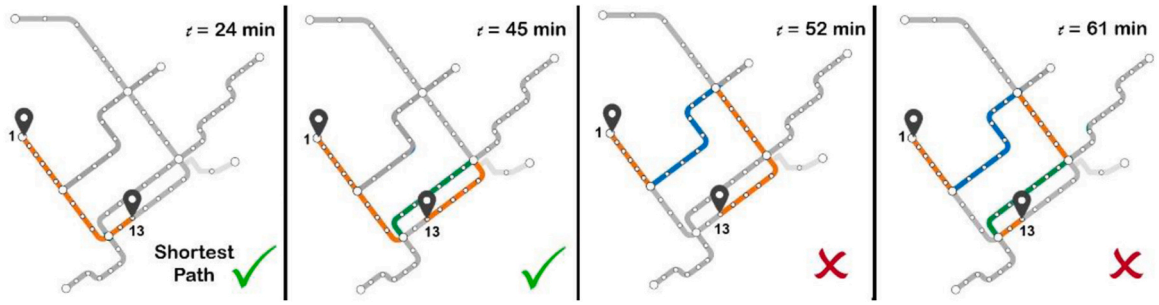

Fig. 7. Quality threshold of route alternatives.

1-Unsatisfied demand caused by physical degradation (denoted by τ_C), as defined in Eq. 21 from earlier sections.

2- Unsatisfied demand caused by decreased route quality (denoted by τ_D), stemming from degradation in travel route quality, as described in Eq. 25.

The employed indicators to assess redundancy are as follow:

$$\overline{R_t} = \frac{\sum^{D_i} R_t}{T_i^A + T_i^B} \tag{22}$$

$$\overline{R_p} = \frac{\sum^{D_i} R_p}{T_i^A + T_i^B} \tag{23}$$

$$\overline{R_u} = \frac{\sum^{D_i} R_u}{T_i^A + T_i^B} \tag{24}$$

$$\tau_D = \frac{T_i^D}{T_i^A + T_i^B} \times 100 \tag{25}$$

Where T_i^D is the number of trips that could not be completed after the i^{th} disruption because of the insufficient quality of alternative routes.

5.3.3. Vulnerability analysis

Normal state

Using the OD data and developed routing algorithms, we found that for 14 % of the trips, theoretical redundancy equals 1 (no alternative is available), and that for around 86 % of trips the theoretical redundancy is greater than 1. However, when considering the quality of the alternatives, it is seen that for 59 % of trips, the acceptable redundancy equals 1 (there is no alternative). The corresponding percentages of trips with one, two, and three acceptable alternatives in the network are 16 %, 21 %, and 4 % respectively. Fig. 8 provides more details.

The results show that the theoretical redundancy ($\overline{R_t}$) in the normal state is 2.97, the acceptable redundancy ($\overline{R_p}$) is 1.70, and the unacceptable redundancy ($\overline{R_u}$) is 1.27. It is also obvious that since all the demand is satisfied in the normal state, both τ_C and τ_D equal 0.

After the disruption

Fig. 6-**j** illustrates that $\overline{R_t}$ is highly sensitive to targeted disruptions. In Targeted Failure Scenario (TFS), following the initial disruption, the theoretical redundancy decreased to 1, indicating that no route alternatives could be identified for OD pairs after subsequent disruptions ($\overline{R_t}$=$\overline{R_p}$=1, and $\overline{R_u}$=0). In Pessimistic Random Failure Scenario (PRFS) and Optimistic Random Failure Scenario (ORFS), a significant reduction in theoretical redundancy was observed after the first disruption, indicating that many trips lost their alternative routes. Specifically, in PRFS, after the third random disruption, and in ORFS, after the fifth random disruption, the network ceased to provide any alternative routes to users.

Conversely, in Realistic Random Failure Scenario (RRFS), although Corresponding Disruption Number to the Annihilation of the Network (CDNAN) value in this scenario was lower than in ORFS, the first substantial decrease in theoretical redundancy occurred

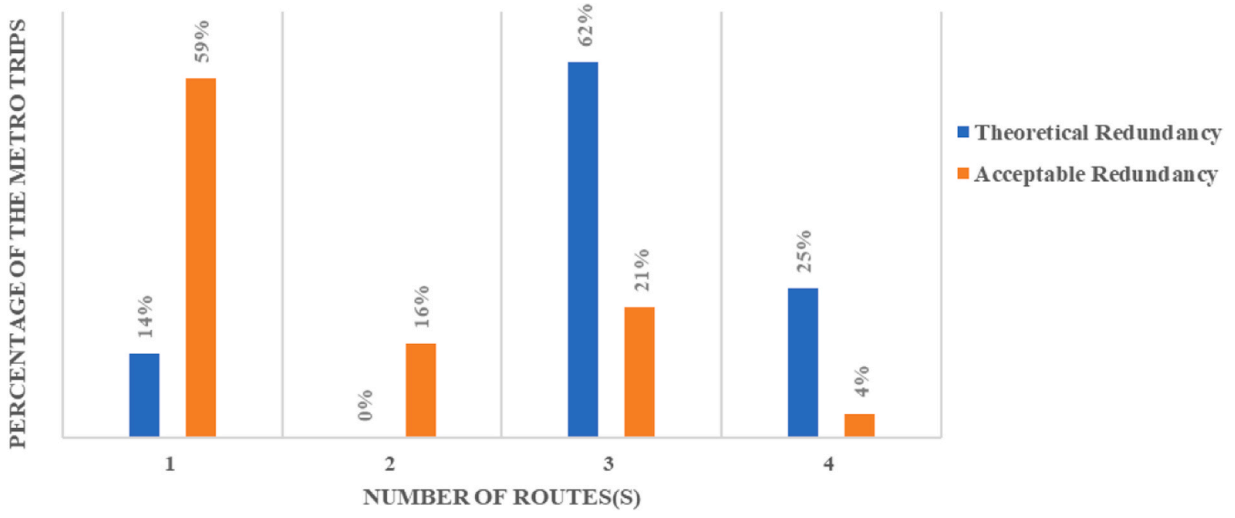

Fig. 8. Distribution of theoretical and acceptable routes in normal state.

after the fourth disruption, with the network able to provide alternative routes up until the eighth disruption.

Notably, contrary to previous analyses, the network exhibited greater vulnerability in ORFS compared to RRFS, suggesting that there is no significant relationship between CDNAN and network vulnerability from a redundancy perspective. Therefore, additional investigation into factors such as the location of disrupted stations and the geometric configuration of the network post-disruption is warranted.

As Fig. 9 indicates, the Montreal UMN contains three cycles: C#1 (7→11→15→18→24→35→7), C#2 (7→11→52→18→24→35→7), and C#3 (11→15→18→52→11). In TFS, the first selected station (Berri-UQAM: station#18) is strategically located at the connection of 3 out of 4 lines. Based on BBFS, by removing this station, 25 % of stations are out of service, and the residual graph is a non-cyclic graph. Therefore, based on graph theory, the network has become a tree that cannot provide any route alternative between two nodes.

In PRFS, the first disrupted station is Snowdon (station #7), impacting 18 % of stations and causing the elimination of cycles C1 and C2, significantly reducing theoretical redundancy. Conversely, in ORFS, station #33 (Université-de-Montréal) is the initial disrupted station, resulting in a mere 5 % physical degradation but leading to the loss of cycles C1 and C2 in the network. While in RRFS, we see that after the 3rd disruption (when stations #39 (Fabre), #31 (Montmorency), and #2 (Du College) are removed and physical degradation is around 15 %), still retains three cycles without a substantial decrease in theoretical redundancy. However, after the fourth disruption (when station #49 (Atwater) is disrupted), two cycles (C2 and C3) are lost, and the theoretical redundancy considerably decreased.

Fig. 6-**k** demonstrating acceptable redundancy, reveals that in TFS, $\overline{R_p}$ decreased to 1 after the first disruption and remained unchanged in subsequent disruptions due to the presence of only one route between each OD pair. Similar patterns are observed in PRFS and ORFS during the initial random disruptions. Surprisingly, despite ORFS having a considerably higher CDNAN than PRFS, $\overline{R_p}$ decreases to 1 sooner in ORFS, indicating that acceptable redundancy is not directly related to CDNAN. Notably, RRFS exhibits the highest acceptable redundancy among all scenarios, highlighting that a high CDNAN value does not necessarily ensure greater redundancy. Moreover, focusing on RRFS, it is observed that after the 8th disruption, the average acceptable redundancy drops below 1, suggesting that for certain OD pairs, single theoretical routes fail to meet the defined quality threshold. Table 3 is intended to show more details concerning each scenario.

The key findings of the redundancy-based vulnerability analysis are as follows:

1-The network is significantly more vulnerable to targeted disruptions.

2- Unlike prior vulnerability analyses emphasizing *C.Deg*(%) and CDNAN are the most impactful factors, in redundancy-based analysis, there is no explicit link between the mentioned factors and vulnerability.

3-Using the theorems of graph theory and studying the geometry of the network show that the most impactful factors in network redundancy are the geometric shape of the network (in the normal state) and the location of disrupted stations (if there are disruptions).

6. Conclusion

This research has presented a comprehensive vulnerability analysis of the Montreal Urban Metro Network (UMN). The study not only developed widely used methods such as network-based and serviceability-based approaches but also introduced a new method called the redundancy-based vulnerability method. In the network-based method, two novel connectivity-related indicators, namely P.C and R.C, were introduced to assess station connectivity and network fragmentation compared to the normal state. Additionally, three innovative indicators—theoretical, acceptable, and unacceptable redundancy—were introduced to evaluate the redundancy of the network, taking into account the quality of route alternatives.

Failure scenarios were considered, including one targeted and three random scenarios—pessimistic, realistic, and optimistic—-which were simulated using Block-Based Failure Strategy (BBFS). The results of all analyses, ranging from network-based to serviceability-based and redundancy-based, indicated that the Montreal UMN is significantly more vulnerable to targeted disruptions than random ones. Moreover, it was observed that the difference between targeted and random failure scenarios is more significant in serviceability-based analysis than in other analyses, indicating that functional indicators are more sensitive to the type of disruption than topological, connectivity, and redundancy indicators. When comparing random failure scenarios, it was evident that the smaller

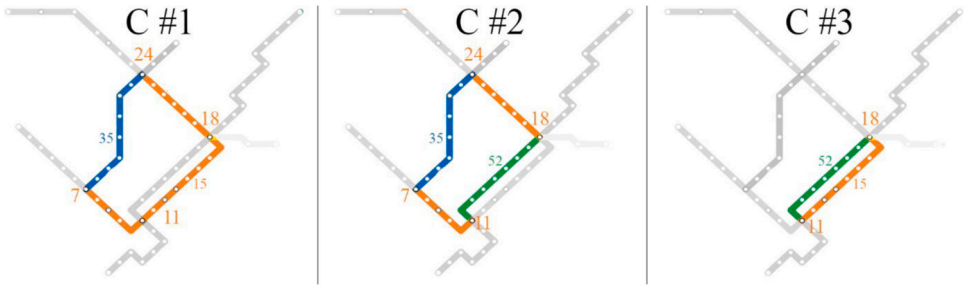

Fig. 9. Cycles in Montreal UMN.

Table 3
Changes of some vulnerability indicators in different failure scenarios.

Disruption Type	Nb. disruptions	$\overline{R_t}$	$\overline{R_p}$	$\overline{R_u}$	*Deg (%)*	τ_C (%)	τ_D (%)	Disruption Type	Nb. disruptions	$\overline{R_t}$	$\overline{R_p}$	$\overline{R_u}$	*Deg (%)*	τ_C (%)	τ_D (%)
Normal State		**2.97**	**1.27**	**1.70**	**0.00**	**0.00**	**0.00**	**Normal State**		**2.97**	**1.27**	**1.70**	**0.00**	**0.00**	**0.00**
TFS	1	1.00	1.00	0.00	25.00	60.58	0.00	**PRFS**	1	1.63	1.37	0.26	14.71	23.68	0.00
	2	1.00	1.00	0.00	47.06	79.98	0.00		2	1.70	1.35	0.35	19.12	32.08	0.00
	3	1.00	1.00	0.00	69.12	94.09	0.00		3	1.72	1.37	0.35	26.47	43.60	0.00
	4	1.00	1.00	0.00	77.94	97.17	0.00		4	1.73	1.37	0.36	30.88	45.84	0.00
	5	1.00	1.00	0.00	80.88	97.59	0.00		5	1.00	0.99	0.01	45.59	58.57	0.79
	6	1.00	1.00	0.00	86.76	98.19	0.00		6	1.00	0.99	0.01	52.94	67.97	1.18
	7	1.00	1.00	0.00	92.65	98.93	0.00		7	1.00	0.99	0.01	60.29	74.40	1.23
	8	1.00	1.00	0.00	97.06	99.76	0.00		8	1.00	1.00	0.00	82.35	98.31	0.00
	9	1.00	1.00	0.00	100.00	100.00	0.00		9	1.00	1.00	0.00	89.71	98.95	0.00
ORFS	1	1.67	1.41	0.25	7.35	12.27	0.48		10	1.00	1.00	0.00	95.59	99.90	0.00
	2	1.62	1.37	0.26	11.76	20.56	0.00		11	1.00	1.00	0.00	100.00	100.00	0.00
	3	1.00	0.98	0.02	14.71	29.38	1.53	**RRFS**	1	2.98	1.70	1.27	4.41	4.27	0.00
	4	1.00	0.98	0.02	20.59	33.99	1.54		2	2.97	1.64	1.33	8.82	13.29	0.00
	5	1.00	0.98	0.02	25.00	41.34	1.75		3	2.96	1.60	1.36	14.71	23.51	0.00
	6	1.00	0.98	0.02	33.82	52.09	2.18		4	1.75	1.19	0.56	19.12	35.08	1.20
	7	1.00	0.96	0.04	39.71	61.22	3.82		5	1.84	1.18	0.66	22.06	37.05	1.56
	8	1.00	0.96	0.04	50.00	69.36	4.18		6	1.84	1.17	0.67	25.00	43.37	1.77
	9	1.00	1.00	0.00	54.41	76.09	0.00		7	1.00	0.90	0.10	30.88	52.44	10.21
	10	1.00	1.00	0.00	58.82	79.11	0.00		8	1.00	0.97	0.03	50.00	68.07	2.64
	11	1.00	1.00	0.00	63.24	84.92	0.00		9	1.00	1.00	0.00	52.94	69.14	0.00
	12	1.00	1.00	0.00	67.65	86.14	0.00		10	1.00	1.00	0.00	64.71	76.98	0.00
	13	1.00	1.00	0.00	72.06	87.27	0.00		11	1.00	1.00	0.00	69.12	83.34	0.00
	14	1.00	1.00	0.00	75.00	90.06	0.00		12	1.00	1.00	0.00	79.41	96.37	0.00
	15	1.00	1.00	0.00	79.41	93.70	0.00		13	1.00	1.00	0.00	86.76	99.06	0.00
	16	1.00	1.00	0.00	83.82	94.90	0.00		14	1.00	1.00	0.00	92.65	99.68	0.00
	17	1.00	1.00	0.00	88.24	98.61	0.00		15	1.00	1.00	0.00	92.65	99.68	0.00
	18	1.00	1.00	0.00	88.24	98.61	0.00		16	1.00	1.00	0.00	94.12	99.80	0.00
	19	1.00	1.00	0.00	91.18	99.31	0.00		17	1.00	1.00	0.00	100.00	100.00	0.00
	20	1.00	1.00	0.00	91.18	99.31	0.00								
	21	1.00	1.00	0.00	97.06	99.88	0.00								
	22	1.00	1.00	0.00	100.00	100.00	0.00								

the value of the Corresponding Disruption Number to the Annihilation of the Network (CDNAN), the greater the network's vulnerability. Thus, the network was more vulnerable to the Pessimistic Random Failure Scenario (PRFS) than the Realistic Random Failure Scenario (RRFS) and was more vulnerable to RRFS than the Optimistic Random Failure Scenario (ORFS). Changes in vulnerability indicators were most significant during the initial disruptions of the failure scenarios, highlighting that the first disruptions have the most impact. This effect was more noticeable in the Targeted Failure Scenario (TFS) than in random scenarios and in functional indicators than in other categories of indicators. Generally, there was a correlation between changes in vulnerability indicators and CDNAN: the larger the CDNAN in a scenario, the lower the rate of change for indicators during the initial disruptions. However, there was a different trend in redundancy-based analysis. The results demonstrated that changes in network redundancy were not sensitive to CDNAN and instead were more sensitive to the location of disrupted stations and the geometric shape of the network.

In this research, our analysis focused exclusively on trips made solely by the metro, omitting users who combined metro travel with other modes such as buses, bike sharing, or carsharing. Future research will incorporate a broader range of travel demand scenarios, including trips where the metro is used either independently or in combination with other modes. This expanded scope will enable us to assess the potential role of different urban transport services, such as buses and bike sharing systems, in mitigating disruptions within the metro system. Additionally, we plan to conduct a detailed socio-demographic study from a microscopic perspective to identify population segments that may be disproportionately affected by disruptions, providing insights into how disruptions impact various user demographics.

The findings of this research offer network operators a fresh perspective for assessing station importance, particularly valuable in crisis situations to prioritize stations for reopening operations. Traditionally, station evaluation focused solely on topological (e.g., centrality) or functional (e.g., passenger volumes) aspects. However, this study underscores the significance of station location and its impact on network geometry, notably in maintaining travel quality. Therefore, in crisis management scenarios, stations that enhance network redundancy (sustaining network cycles) should take precedence in reopening efforts, even over stations with higher traffic but lesser impact on network redundancy, as they contribute to improved travel quality for all passengers. Furthermore, with the introduction of SDCFs and BBFS in this study, network designers are encouraged to integrate the BBFS algorithm into their design processes and strategically plan for SDCFs, considering their limitations in terms of cost, complexity, and construction time, to optimize their location.

CRediT authorship contribution statement

Rezvani Dehaghani Kaveh: Writing – original draft, Software, Methodology, Investigation, Funding acquisition, Formal analysis, Conceptualization. **Morency Catherine:** Writing – review & editing, Supervision, Data curation.

Declaration of Competing Interest

The authors, Kaveh Rezvani Dehaghani and Catherine Morency, declare that they have no known competing financial interests or personal relationships that could have appeared to influence the work reported in this paper.

Data availability

The authors do not have permission to share data.

References

[1] J. Zhang, S. Wang, X. Wang, Comparison analysis on vulnerability of metro networks based on complex network, Phys. A: Stat. Mech. its Appl. 496 (2018) 72–78.
[2] J. Zhang, M. Wang, Transportation functionality vulnerability of urban rail transit networks based on movingblock: the case of Nanjing metro, Phys. A: Stat. Mech. Its Appl. 535 (2019) 122367.
[3] STM, *Société de transport de Montréal.*
[4] L. Hong, et al., Vulnerability assessment and mitigation for the Chinese railway system under floods, Reliab. Eng. Syst. Saf. 137 (2015) 58–68.
[5] L. Sun, et al., Vulnerability assessment of urban rail transit based on multi-static weighted method in Beijing, China, Transp. Res. Part A: Policy Pract. 108 (2018) 12–24.
[6] R. Jiang, Q.-C. Lu, Z.-R. Peng, A station-based rail transit network vulnerability measure considering land use dependency, J. Transp. Geogr. 66 (2018) 10–18.
[7] Y. Zhang, et al., A double-weighted vulnerability assessment model for metrorail transit networks and its application in Shanghai metro, Int. J. Crit. Infrastruct. Prot. 29 (2020) 100358.
[8] F. Ma, et al., Exploring the robustness of public transportation for sustainable cities: A double-layered network perspective, J. Clean. Prod. 265 (2020) 121747.
[9] Y. Meng, et al., Comparison analysis on complex topological network models of urban rail transit: A case study of Shenzhen Metro in China, Phys. A: Stat. Mech. Its Appl. 559 (2020) 125031.
[10] Z. Xu, S.S. Chopra, Network-based Assessment of Metro Infrastructure with a Spatial–temporal Resilience Cycle Framework, Reliab. Eng. Syst. Saf. 223 (2022) 108434.
[11] X. Li, et al., Network-based transportation system analysis: A case study in a mountain city, Chaos, Solitons Fractals 107 (2018) 256–265.
[12] F. Ma, et al., Assessing the vulnerability of urban rail transit network under heavy air pollution: A dynamic vehicle restriction perspective, Sustain. Cities Soc. 52 (2020) 101851.
[13] H. Zhang, Y. Yao, An integrative vulnerability evaluation model to urban road complex network, Wirel. Pers. Commun. 107 (1) (2019) 193–204.
[14] L. Hong, et al., Vulnerability analysis of public transit systems from the perspective of urban residential communities, Reliab. Eng. Syst. Saf. 189 (2019) 143–156.
[15] N. Khademi, M. Bababeik, A. Fani, Sparse rail network robustness analysis: Functional vulnerability levels of accidents resulting from human errors, J. Saf. Sci. Resil. 2 (3) (2021) 111–123.

[16] J. Zhang, et al., Vulnerability assessments of weighted urban rail transit networks with integrated coupled map lattices, Reliab. Eng. Syst. Saf. 214 (2021) 107707.
[17] L.-G. Mattsson, E. Jenelius, Vulnerability and resilience of transport systems–A discussion of recent research, Transp. Res. Part A: Policy Pract. 81 (2015) 16–34.
[18] K. Berdica, An introduction to road vulnerability: what has been done, is done and should be done, Transp. Policy 9 (2) (2002) 117–127.
[19] Ga D'este, M.A. Taylor, Network vulnerability: an approach to reliability analysis at the level of national strategic transport networks, Emerald Group Publishing Limited, 2003.
[20] K. Berdica, L.-G. Mattsson, Vulnerability: a model-based case study of the road network in Stockholm. in *Critical infrastructure*, Springer, 2007, pp. 81–106.
[21] E. Jenelius, L.-G. Mattsson, Road network vulnerability analysis of area-covering disruptions: A grid-based approach with case study, Transp. Res. Part A: Policy Pract. 46 (5) (2012) 746–760.
[22] M. Taylor, Vulnerability analysis for transportation networks, Elsevier, 2017.
[23] J. Zhang, Z.-H. Zhang, A Review of the Research Methods on Vulnerability of Transportation System, CICTP 2019 (2019) 4294–4305.
[24] S. Pan, et al., Vulnerability and resilience of transportation systems: A recent literature review, Phys. A: Stat. Mech. its Appl. 581 (2021) 126235.
[25] L. Mussone, V.J.A. Salgado, R. Notari, Evaluation of robustness in underground networks, Phys. A: Stat. Mech. Its Appl. 651 (2024) 130014.
[26] J. Zhang, et al., Robustness assessments of urban rail transit networks based on user equilibrium with time compensation mechanism, Phys. A: Stat. Mech. its Appl. 613 (2023) 128530.
[27] Z. Du, et al., Identifying critical nodes in metro network considering topological potential: A case study in Shenzhen city—China, Phys. A: Stat. Mech. Its Appl. 539 (2020) 122926.
[28] J. Song, et al., Assessment and solutions for vulnerability of urban rail transit network based on complex network theory: A case study of Chongqing, Heliyon 10 (5) (2024).
[29] C. Von Ferber, et al., Public transport networks: empirical analysis and modeling, Eur. Phys. J. B 68 (2) (2009) 261–275.
[30] R. Jain, G. Purohit, Page ranking algorithms for web mining, Int. J. Comput. Appl. 13 (5) (2011) 22–25.
[31] M.R. Prajapati, A survey paper on hyperlink-induced topic search (HITS) algorithms for web mining, Int J. Eng. 1 (2) (2012) 8.
[32] X. Liu, Z. Lei, Z. Duan, Assessing metro network vulnerability with turn-back operations: A Monte Carlo method, Phys. A: Stat. Mech. its Appl. 646 (2024) 129923.
[33] G.-H. Tzeng, J.-J. Huang, Multiple attribute decision making: methods and applications, CRC press, 2011.
[34] C.E. Shannon, A mathematical theory of communication, Bell Syst. Tech. J. 27 (3) (1948) 379–423.
[35] M. Rubinov, O. Sporns, Complex network measures of brain connectivity: uses and interpretations, Neuroimage 52 (3) (2010) 1059–1069.
[36] E. Drrksrra, no. l, A Note two Probl. Connex. Graphs 959 (1959) 269–271.
[37] A. Kermanshah, S. Derrible, A geographical and multi-criteria vulnerability assessment of transportation networks against extreme earthquakes, Reliab. Eng. Syst. Saf. 153 (2016) 39–49.